Femtosecond Time-Resolved Absorption Spectroscopy of Main-Form and High-Salt Peridinin−Chlorophyll *a*−Proteins at Low Temperatures†

Robielyn P. Ilagan,‡ Jeremy F. Koscielecki,‡ Roger G. Hiller,§ Frank P. Sharples,§ George N. Gibson,|| Robert R. Birge,‡ and Harry A. Frank*,‡

Department of Chemistry, University of Connecticut, Storrs, Connecticut 06269-3060, Biology Department, Macquarie University, NSW 2109, Australia, and Department of Physics, University of Connecticut, Storrs, Connecticut 06269-3046

Received June 19, 2006; Revised Manuscript Received August 16, 2006

ABSTRACT: Steady-state and femtosecond time-resolved optical methods have been used to compare the spectroscopic features and energy transfer dynamics of two systematically different light-harvesting complexes from the dinoflagellate *Amphidinium carterae*: main-form (MFPCP) and high-salt (HSPCP) peridinin−chlorophyll *a*−proteins. Pigment analysis and X-ray diffraction structure determinations [Hofmann, E., Wrench, P. M., Sharples, F. P., Hiller, R. G., Welte, W., Diederichs, K. (1996) *Science 272*, 1788−1791; T. Schulte, F. P. Sharples, R. G. Hiller, and E. Hofmann, unpublished results] have revealed the composition and geometric arrangements of the protein-bound chromophores. The MFPCP contains eight peridinins and two chlorophyll (Chl) *a*, whereas the HSPCP has six peridinins and two Chl *a*, but both have very similar pigment orientations. Analysis of the absorption spectra has shown that the peridinins and Chls absorb at different wavelengths in the two complexes. Also, in the HSPCP complex, the Q_y transitions of the Chls are split into two well-resolved bands. Quantum computations by modified neglect of differential overlap with partial single and double configuration interaction (MNDO-PSDCI) methods have revealed that charged amino acid residues within 8 Å of the pigment molecules are responsible for the observed spectral shifts. Femtosecond time-resolved optical spectroscopic kinetic data from both complexes show ultrafast (<130 fs) and slower (∼2 ps) pathways for energy transfer from the peridinin excited singlet states to Chl. The Chl-to-Chl energy transfer rate constant for both complexes was measured and is discussed in terms of the Förster mechanism. It was found that, upon direct Chl excitation, the Chl-to-Chl energy transfer rate constant for MFPCP was a factor of 4.2 larger than for HSPCP. It is suggested that this difference arises from a combination of factors including distance between Chls, spectral overlap, and the presence of two additional peridinins in MFPCP that act as polarizable units enhancing the rate of Chl-to-Chl energy transfer. The study has revealed specific pigment−protein interactions that control the spectroscopic features and energy transfer dynamics of these light-harvesting complexes.

Peridinin−chlorophyll *a*−protein (PCP)[1] is a water-soluble complex from the dinoflagellate *Amphidinium carterae* that exhibits a very high (>95%) peridinin-to-chlorophyll energy transfer efficiency (*1*−*4*). The crystal structure of PCP at 2.0 Å resolution shows a trimeric subunit arrangement where the minimal unit of the complex is composed of eight peridinins and two chlorophyll (Chl) *a* molecules noncovalently bound to a 32 kDa protein (Figure 1) (*5*). The peridinin molecules are assembled in two clusters of four, each surrounding and in van der Waals contact with one Chl *a*. The closest approach between the conjugated π-electron chain of the peridinins and the tetrapyrrole rings of Chl is 3.3−3.8 Å. The center-to-center distance between the two Chls within a subunit is 17.4 Å, and the shortest distance between Chls in neighboring subunits is ∼40 Å.

The PCP complex has been the subject of absorption, fluorescence, linear and circular dichroism, two-photon excitation, nonlinear polarization, and transient optical spectroscopic investigations at room and cryogenic temperatures (*3*, *4*, *6*−*15*). This work has explored the electronic excited states of the bound peridinins, the nature of the interactions between peridinin and Chl *a* molecules, and the dynamics and efficiency of energy transfer. Also, quantum mechanical calculations have made use of the published coordinates of the PCP to explore the nature of the excited states of the bound pigments, to correlate with spectroscopic observables, and to determine the energy transfer mechanism

† This work was supported by grants from the National Institutes of Health (GM-30353 to H.A.F. and GM-34548 to R.R.B.), the University of Connecticut Research Foundation, and the National Science Foundation (BES-0412387, CCF-0432151 to R.R.B.) and by a Macquarie University research development grant (to R.G.H). The laser system was purchased by a grant from the National Science Foundation (MRI-0320403 to G.N.G., R.R.B., and H.A.F.).

* Corresponding author: Department of Chemistry, 55 North Eagleville Rd., University of Connecticut, Storrs, CT 06269-3060; tel 860-486-2844; fax 860-486-6558; e-mail harry.frank@uconn.edu.

‡ Department of Chemistry, University of Connecticut.

§ Macquarie University.

|| Department of Physics, University of Connecticut.

[1] Abbreviations: MFPCP, main-form peridinin−chlorophyll *a*−protein; HSPCP, high-salt peridinin−chlorophyll *a*−protein; Chl, chlorophyll; MNDO−PSDCI, modified neglect of differential overlap with partial single and double configuration interaction; MM2, molecular mechanics 2; ONIOM, *n*-layered integrated molecular orbital method; CI, configuration interaction; MO, molecular orbital; CISD, configuration interaction single and double; EADS, evolution-associated difference spectra; ND, nondecaying; 2-MTHF, 2-methyltetrahydrofuran; LH2, light-harvesting 2 complex from purple photosynthetic bacteria.

10.1021/bi061217u CCC: $33.50
Published on Web 10/10/2006

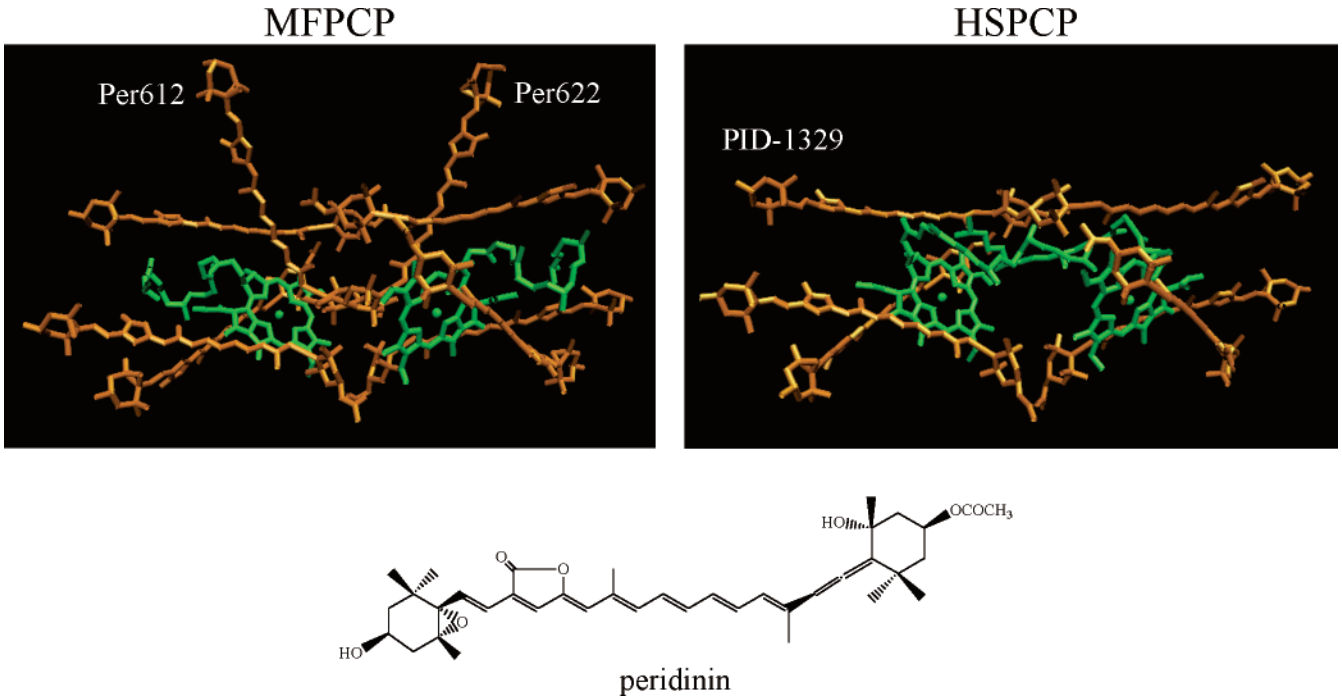

FIGURE 1: (Top) Structures of the pigments in a monomeric subunit of the MFPCP and HSPCP complexes. The coordinates were taken from Protein Data Bank (PDB) codes 1PPR for MFPCP and 2C9E for HSPCP. A monomeric subunit of the MFPCP complex has eight peridinin and two Chl *a* molecules. The HSPCP complex has six peridinin and two Chl *a* molecules. (Bottom) Structure of peridinin.

and pathways that ultimately lead to energy trapping in photosystem II (*14*−*19*). The spectroscopic studies and quantum mechanical calculations indicate the eight peridinins and two Chl *a* molecules in the complex are inhomogeneous and occupy binding sites with different energies (*4*, *10*, *11*, *15*, *17*). MNDO-PSDCI calculations on geometry-optimized peridinin suggested that two peridinins, Per612 and Per622 (Figure 1), have blue-shifted absorption spectra compared to the other six and also have reordered excited singlet states (*15*). This reordering was postulated to result in enhanced energy transfer from the two blue-shifted peridinins to other peridinins rather than directly to Chl (*15*).

The above description pertains to the main form of PCP, but another form of PCP from *A. carterae* has been identified from purification by cation-exchange column chromatography and a linear salt gradient (*20*). After elution of the dominant main-form PCP (MFPCP), a minor component comprising ∼2% of the total PCP was collected at high salt concentration. This complex is referred to as the high-salt PCP (HSPCP). The two complexes, MFPCP and HSPCP, are distinguished from each other by differences in absorption, fluorescence, and circular dichroism spectra, pigment composition, molar mass, antigenicity, and amino acid sequence (*20*).

The absorption spectra of the MFPCP and HSPCP complexes exhibit several distinguishing features that are evident at cryogenic temperatures (*4*). The 10 K absorption spectrum of the HSPCP complex shows more pronounced vibrational structure in the peridinin absorption region than does the MFPCP complex. In addition, the Q_y transitions of the Chls bound in the HSPCP complex are split into two well-resolved bands indicating structural heterogeneity in the Chl binding sites, but the structural basis for this is unknown (*4*). Steady-state fluorescence excitation spectroscopy reveals >95% peridinin-to-Chl *a* energy transfer efficiency in the HSPCP complex, which is similar to that observed for MFPCP (*4*, *20*). Pigment analysis shows that the HSPCP complex accomplishes this with only six peridinins and two Chl *a* compared to eight peridinins and two Chl *a* in MFPCP (*20*). Also, the HSPCP protein has a molecular mass of 34 kDa, compared to 32 kDa for MFPCP, and the amino acid sequences of the MFPCP and HSPCP complexes are 31% identical and 55% similar with different numbers of charged amino acid residues. There are 11 arginine (Arg), 29 lysine (Lys), 18 glutamic acid (Glu), and 21 aspartic acid (Asp) residues in the HSPCP, whereas in the MFPCP there are 3 Arg, 27 Lys, 10 Glu, and 24 Asp. The elution of the HSPCP complex from a cation-exchange column at pH 5.0 and higher salt concentration relative to MFPCP can be attributed to the larger number of positively charged amino acid residues.

The crystal structure of the HSPCP complex has recently been reported and has revealed the arrangement of the six bound peridinins and two Chl *a* molecules (T. Schulte, F. P. Sharples, R. G. Hiller, and E. Hofmann, unpublished results). The structure of the HSPCP complex is very similar to that of the MFPCP, but there are some notable differences. The HSPCP lacks the peridinin equivalents of Per612 and Per622 in the MFPCP (Figure 1), and the center-to-center distance between the two Chl *a* molecules is 18.4 Å, compared to 17.4 Å in MFPCP. In HSPCP the Chl phytol tails reside between the two Chls in the space occupied by Per612 and Per622 in the MFPCP (Figure 1).

Peridinin itself is a uniquely substituted carotenoid with a C_{37} carbon skeleton (Figure 1) rather than the typical C_{40} system present in most carotenoids (*21*). Also, peridinin possesses an allene group and a lactone ring in conjugation with the π-electron conjugated system and epoxy and acetate functional groups (Figure 1). Although peridinin has no symmetry, its spectroscopic behavior has characteristics of

an idealized C_{2h} symmetric system, and many of its properties can be described by use of symmetry-based selection rules involving two low-lying singlet excited states denoted S_1 ($2^1A_g^-$) and S_2 ($1^1B_u^+$). The transition by one-photon absorption from the ground state S_0, also having A_g^- symmetry, to the lowest excited S_1 ($2^1A_g^-$) state is forbidden, whereas the transition to the excited S_2 ($1^1B_u^+$) state is strongly allowed and appears in the visible region. Because the fluorescence emission spectrum of peridinin exhibits a large Stokes shift relative to the strong S_0 ($1^1A_g^-$) $\rightarrow$ S_2 ($1^1B_u^+$) absorption band, its origin has been assigned to the lowest excited singlet state, S_1 ($2^1A_g^-$) (*6*, *22*−*25*). This assignment is consistent with many reports showing carotenoids with π-electron conjugated systems shorter than $N = 9$ have dominant emission from S_1 (*22*, *26*−*33*).

Peridinin is unusual among carotenoids in that its excited-state absorption spectrum and dynamics exhibit a pronounced solvent dependence. In nonpolar to moderately polar solvents, there are bands at ~520 and ~650 nm in the excited-state absorption spectrum of peridinin, whereas a single broad band at ~590 nm is observed in polar solvents (*22*). The S_1 lifetime of peridinin is also strongly dependent on solvent environment, with values ranging from 7 ps in the strongly polar solvent trifluoroethanol to 172 ps in the nonpolar solvents cyclohexane and benzene (*22*). To account for these effects, the presence of an intramolecular charge-transfer (S_{ICT}) state was invoked, and the long-wavelength features of the excited-state spectra were assigned to an $S_{ICT} \rightarrow S_2$ transition (*22*). Subsequent investigations (*23*) identified the carbonyl group conjugated to the polyene chain as responsible for the dependence of the spectra and dynamics on solvent polarity.

Further spectroscopic experimentation and quantum mechanical calculations have explored the nature of the postulated S_{ICT} state (*15*, *16*, *34*). MNDO-PSDCI calculations suggested that the S_1 state has a large dipole moment in both polar and nonpolar environments and that S_1 is the actual charge transfer state (*15*). In contrast, quantum calculations using time-dependent density functional theory under the Tamm−Dancoff approximation indicated that the S_{ICT} state is a distinct state that lies below S_1 in polar solvents and remains above the S_1 state in nonpolar solvents (*16*). Spectroscopic studies have suggested that the S_{ICT} state of peridinin is a separate state that can act as an efficient energy donor to Chl *a* in the PCP complex (*8*, *34*). This idea has been supported by recent pump-dump-probe spectroscopic experiments, which suggest that S_1 and S_{ICT} are distinct but interconnected states (*34*). However, these results are not inconsistent with a model whereby the S_{ICT} state evolves from S_1 and where the short-wavelength (~520 nm) excited-state spectroscopic features are associated with the $S_1 \rightarrow S_n$ transition and the long-wavelength (~650 nm) features correspond to the $S_{ICT} \rightarrow S_n$ transition (*23*).

In this study we compare the femtosecond time-resolved spectroscopic properties and energy transfer dynamics of the MFPCP and HSPCP complexes at cryogenic temperatures where the spectral features are better resolved than spectra taken at room temperature. The systematic alteration in the structures and pigment compositions of these two complexes provides a valuable means of exploring the controlling factors for efficient energy transfer in photosynthetic light-harvesting complexes.

MATERIALS AND METHODS

Sample Preparation. The PCP complexes were isolated from *A. carterae* as described by Sharples et al. (*20*). After purification, the complexes were suspended in 50 mM Tricine/20 mM KCl buffer, pH 7.5, containing 60% glycerol (Sigma) for the 10 K experiments. The optical density of the samples was adjusted to approximately 0.4 at the maximum of the peridinin absorption in a 4 mm path length polymethacrylate plastic cuvette. Peridinin was isolated from the MFPCP complex and purified as described by Shima et al. (*15*). The purified peridinin was dissolved in 2-methyltetrahydrofuran (2-MTHF) and its optical density was adjusted to 0.3 at the excitation wavelength. Absorption spectra of the samples were taken at room temperature before and after the transient absorption measurements to confirm sample integrity.

Transient Absorption Spectroscopy. Transient absorption spectroscopy was performed at 10 K or 77 K by use of a Janis helium vapor flow STVP-100 cryostat. The ultrafast transient absorption spectrometer has been described in detail previously (*35*). The samples were excited with a pump laser excitation energy of 1 μJ/pulse. The instrument response function was determined to be 130 ± 45 fs based on the values obtained from global fitting. Transient absorption datasets were analyzed with the ASUfit program, provided by Dr. Evaldas Katilius, and Surface Xplorer Pro software v. 1.0.4 (Ultrafast Systems LLC). The data were corrected for dispersion by subtracting a curve of time zero (t_0) values obtained from fitting the kinetics at different wavelengths.

Ground-State Optimization Computations. Calculation of the spectroscopic properties of the peridinin and chlorophyll chromophores within HSPCP requires minimization of these chromophores inside the protein binding sites. ChemBats3D (CambridgeSoft, Cambridge, MA) was used to add hydrogen atoms, with the assumption that all residues were neutral except for glutamic and aspartic acid residues (negative) and lysine and arginine residues (positive). Hydrogen atoms were minimized by using the MM2 force field with simulated annealing and slow (10 K/ps) temperature ramping following the temperature sequence 0-300-0-300-0 K. The hydrogen atoms were then further minimized by use of MOZYME and the PM5 Hamiltonian (MopacUltra, CambridgeSoft, Cambridge, MA). All non-hydrogen atoms were held fixed during both the mechanical and quantum mechanical optimizations. The peridinin and chlorophyll molecules were then minimized within the binding sites by using PM5. Previous studies have shown that PM5 provides a reliable treatment of chlorophylls and generates geometries and charge distributions in good agreement with higher-level density functional methods (*36*). However, we found that PM5 calculations did not generate a ground-state geometry that yielded good MNDO−PSDCI spectroscopic properties. Previous studies have shown the MNDO-PSDCI methods provide fairly accurate spectroscopic properties of porphyrins and chlorins when they are based on B3LYP/6-31G(d) minimized ground states (*37*, *38*). Thus, we optimized the two chlorophyll chromophores within the protein binding site by use of B3LYP/6-31G(d) density functional theory (*39*) and ONIOM methods (*40*, *41*) to handle the protein matrix.

Spectroscopic Computations. The excited singlet-state properties of the peridinin and chlorophyll chromophores

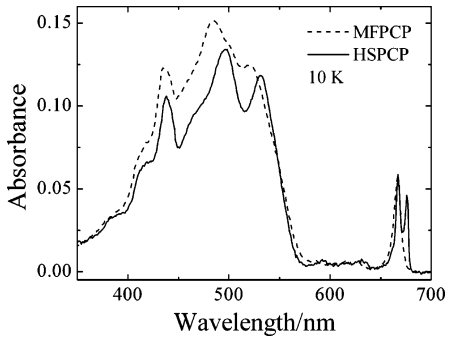

FIGURE 2: Steady-state absorption spectra of the MFPCP and HSPCP complexes taken at 10 K. The spectra were normalized to the most prominent Chl Q_y band of the complexes.

were calculated by MNDO-PSDCI methods (*15*, *38*, *42*−*44*). Survey calculations on the peridinin chromophores were carried out with full single and double CI within the six highest energy occupied and six lowest energy unoccupied π MOs. Final calculations reported here on PID-1329 were carried out with 8 × 8 CISD (64 singles and 2080 doubles). The binding site was represented by the first shell of residues and all charged residues within 8 Å. The calculations on the two chlorophyll chromophores (CL2-1327 and CL2-1328) were carried out with full single and double CI within the eight highest energy occupied and eight lowest energy unoccupied π MOs. To make the calculation more tractable, the long alkyl chain attached to R17 was replaced with a single methyl group, as a survey calculation indicated that such a replacement had no impact on the CISD results other than to speed up the calculation. All charged, or potentially charged, residues near the chlorophylls were included in the calculations, but only those charged residues within 8 Å had an observable effect.

RESULTS

Steady-state absorption spectra of the MFPCP and HSPCP complexes taken at 10 K are shown in Figure 2. In both complexes, peridinin absorbs from 450 to 550 nm and chlorophyll (Chl) absorbs at ∼435 (Soret) and at ∼670 nm (Q_y region). A splitting of the Chl Q_y bands of the HSPCP complex at 10 K was observed as previously reported and is attributed to different site energies of the two Chls (*4*). Gaussian deconvolution of the Chl Q_y region of the MFPCP complex also indicates that upon lowering the temperature to 10 K, the two Chls occupy sites with dissimilar energies but the Q_y bands are not spectrally resolved (*4*).

Transient absorption spectra of the MFPCP and HSPCP complexes taken at 10 K at different delay times with 530 nm excitation are shown in Figure 3. Excitation at 480 and 500 nm produced virtually identical spectral profiles (data not shown). At a delay time of 0.0 ps, that is, during the excitation laser pulse, the transient absorption spectrum of MFPCP (Figure 3A) showed bleaching of the ground-state peridinin absorption band at ∼550 nm and also a broad excited-state peridinin absorption signal ranging from 560 to 725 nm. This signal is due to both $S_1 \rightarrow S_n$ and $S_{ICT} \rightarrow S_n$ transitions. For convenience we shall sometimes refer to this combination of spectroscopic transitions as $S_{1/ICT} \rightarrow S_n$. At this same early time delay, an onset of Chl Q_y band bleaching at 669 nm was observed, suggesting that energy is transferred from the S_2 state of peridinin to Chl. In going from time

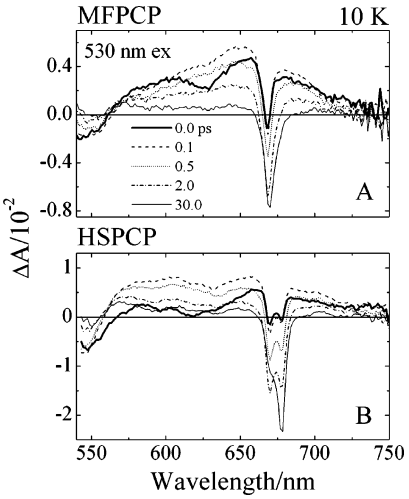

FIGURE 3: Transient absorption spectra taken at 10 K of (A) MFPCP and (B) HSPCP at different delay times from 0.0 to 30.0 ps. The complexes were excited at 530 nm.

zero to a delay time of 0.1 ps, an increase in the peridinin excited-state absorption was observed, indicating that S_2 relaxation, which populates both the S_1 and S_{ICT} states, is occurring in this time range. At this delay time the spectrum has a well-formed maximum at 650 nm. As time elapses from 0.5 to 2.0 ps, both the broad excited-state absorption and the bleaching of the ground-state absorption of peridinin decrease and the bleaching in the Chl Q_y region increases, indicating energy transfer is occurring from peridinin to Chl. At a delay time of 30.0 ps, the transient absorption spectrum is dominated by Chl Q_y bleaching at 670 nm, indicating the transfer from peridinin is essentially complete. Upon close inspection of Figure 3A, it is observed that in the earliest time trace of the MFPCP complex, the Chl Q_y band bleaching appears at 669 nm, but then red-shifts by 1 nm as time elapses from 0.0 to 30.0 ps. As will be discussed in more detail below, this is indicative of energy transfer between the two Chls.

Upon excitation of the HSPCP complex at 530 nm, an instantaneous onset of bleaching of the peridinin absorption and of both Chl Q_y absorption bands at 670 and 678 nm was observed (Figure 3B), indicating very rapid energy transfer from the S_2 state of peridinin to Chl. Once again, the broad positive signal from 560 to 750 nm is due to peridinin $S_{1/ICT} \rightarrow S_n$ excited-state absorption that overlaps the Chl Q_y band bleaching between 660 and 690 nm. However, in HSPCP the transient absorption of peridinin in the 560−750 nm range is much flatter and broader than in the MFPCP complex. Similar to the behavior of MFPCP, the HSPCP complex also exhibits a decrease in both peridinin $S_{1/ICT} \rightarrow S_n$ excited-state absorption and ground-state absorption bleaching as time elapses from 0.5 to 2.0 ps. In addition to the decay of these absorption signals, a parallel increase in the bleaching of both Chl Q_y bands occurs, indicating that energy is transferred from peridinin to both Chls. At the 30.0 ps delay time, the $S_{1/ICT} \rightarrow S_n$ absorption in HSPCP is minimal, suggesting that energy transfer from peridinin to Chl is for the most part complete as it is in the MFPCP complex. Also, in going from the 2.0 ps to the 30.0 ps delay time, the Chl bleaching at 670 nm decreases substantially while the Chl bleaching at 678 nm increases and persists for a long time. This is indicative of energy transfer from

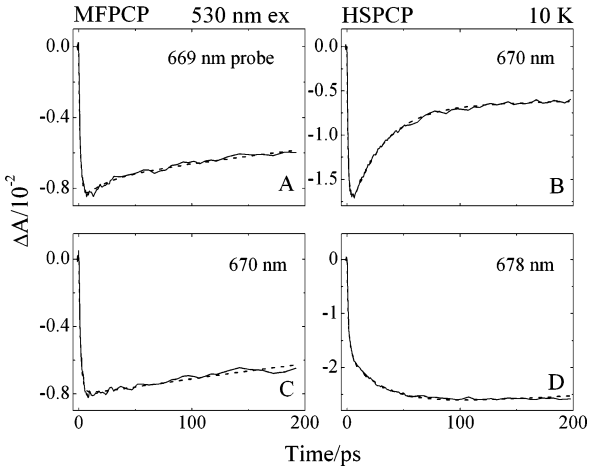

FIGURE 4: Kinetic traces measured at 10 K of (A,C) MFPCP and (B,D) HSPCP with excitation at 530 nm. The probe wavelengths specified in the figures were in the region of Chl Q_y band bleachings, 669 and 670 nm for MFPCP and 670 and 678 nm for HSPCP.

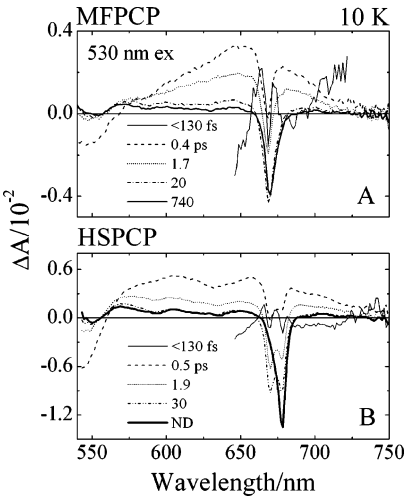

FIGURE 5: Evolution-associated difference spectra (EADS) for (A) MFPCP and (B) HSPCP from global fitting analysis of data sets obtained from complexes excited in the peridinin absorption region at 530 nm.

the short-wavelength-absorbing Chl to the long-wavelength-absorbing Chl.

Global fitting of the kinetic data sets was accomplished by use of a sequential kinetic scheme with increasing lifetimes. This procedure yields evolution-associated difference spectra (EADS), where the time constants of the processes may correspond to the lifetimes of the transient species, but the spectral profiles do not necessarily represent the pure excited-state spectra of the molecules (*45*). The quality of the global fits and the number of decay components necessary to reproduce the experimental data were evaluated by minimization of the χ^2 factor and inspection of the flatness of a residual matrix array. Representative time traces at specific probe wavelengths are given in Figure 4, and the amplitude spectra resulting from the global fits are shown in Figure 5. The kinetic traces at the Chl Q_y band bleaching, 669 nm for MFPCP (Figure 4A) and 670 nm for HSPCP (Figure 4B), exhibit a rapid build-up and partial recovery of the bleaching signal. This suggests that the short-wavelength-absorbing Chl is transferring its energy to the long-wavelength-absorbing Chl. This is confirmed in the 678 nm probe time response for the HSPCP complex (Figure 4D), where the rise of the bleaching at 678 nm displays the same dynamics as the decay of the bleaching at 670 nm (Figure 4B). The kinetic trace at 670 nm (Figure 4C) for the MFPCP complex also shows a low-amplitude long-time constant (~740 ps) recovery of the bleaching signal. This recovery is most likely due to equilibration or annihilation between the two Chls (*8*, *9*, *46*). For both complexes, the kinetic traces at the long wavelengths (Figure 4C,D) show nondecaying bleachings that are due to the relatively long (~5 ns) lifetime of the Chl *a* excited state (*2*).

The EADS amplitude spectra resulting from the global fits of the data from both complexes are presented in Figure 5 and display a first component having a lifetime <130 fs and consisting of a very broad negative band from 550 to 650 nm due to stimulated emission from peridinin (partially deleted from Figure 5 for clarity). Also observed in this component is a small amount of bleaching of the Chl Q_y band at 669 nm for MFPCP and at 670 and 678 nm for HSPCP. Chl bleaching appears in the first EADS component and both Chl Q_y bands are bleached, supporting the notion that, during the laser pulse into the peridinin absorption region, energy is being transferred from the S_2 state of peridinin to both Chls. The first EADS is followed by a second component having a 0.4 ± 0.2 ps (MFPCP) or 0.5 ± 0.1 ps (HSPCP) lifetime (dashed lines in Figure 5). This component displays a broad amplitude spectrum from 560 to 750 nm, associated with $S_{1/ICT} \rightarrow S_n$ excited-state absorption of peridinin. The spectrum of this component is broader and flatter for the HSPCP complex (Figure 5B) than for the MFPCP complex (Figure 5A), which peaks at 650 nm. An increase in Chl Q_y band bleaching is also seen in this component along with peridinin ground-state bleaching in the wavelength region below 570 nm. The rapid time constant of this component is consistent with vibrational relaxation, but the increase in Chl Q_y band bleaching suggests that energy transfer from upper vibrational levels of the peridinin S_1 or S_{ICT} state to the Chls is occurring. The third EADS in Figure 5 corresponds to a 1.7 ± 0.2 ps (MFPCP) or 1.9 ± 0.2 ps (HSPCP) kinetic component and is characterized by a decrease of both the peridinin bleaching and excited-state $S_{1/ICT} \rightarrow S_n$ absorption. This indicates that peridinin has transferred some of the vibronically relaxed excited-state population to Chl. For MFPCP, a fourth EADS displays a pronounced Chl Q_y band bleaching at 669 nm. For HSPCP, the fourth EADS shows Chl Q_y band bleachings with comparable intensities at 670 and 678 nm. This is evidence that peridinin transfers energy more or less equally to both Chls. The fourth EADS has a 20 ± 5 ps time constant for MFPCP and a 30 ± 2 ps time constant for HSPCP. These are followed by a fifth EADS of a very long (740 ps for the MFPCP) or nondecaying (ND for the HSPCP) component. For the HSPCP, the Q_y band bleaching at 670 nm in the fourth EADS disappears while the bleaching at 678 nm persists in the final nondecaying EADS, indicating Chl-to-Chl energy transfer.

The MFPCP and HSPCP complexes were also excited in the Chl Q_y region at 660 nm to investigate direct Chl-to-Chl energy transfer. The EADS resulting from the global fitting are shown in Figure 6. For both complexes, the transient absorption data were best fit with two components. The first EADS component shows Chl Q_y band bleaching at 669 nm

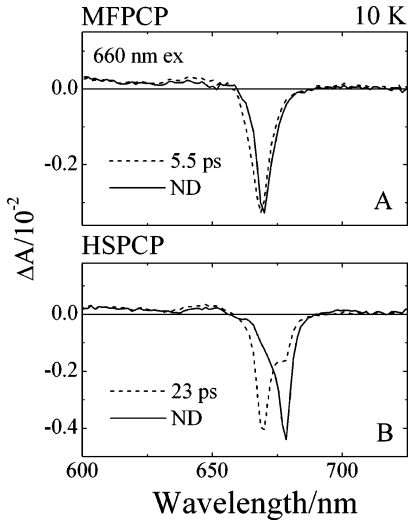

FIGURE 6: Evolution-associated difference spectra (EADS) for (A) MFPCP and (B) HSPCP from global fitting analysis of data sets obtained from complexes excited in the Chl Q_y region at 660 nm.

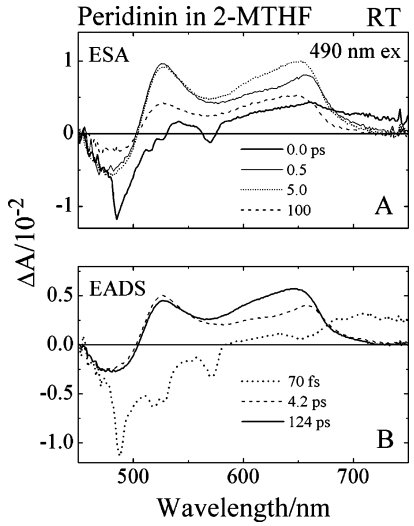

FIGURE 7: (A) Transient absorption spectra of peridinin in 2-MTHF excited at 490 nm at room temperature at different delay times from 0.0 to 100 ps. (B) Evolution-associated difference spectra (EADS) for peridinin in 2-MTHF obtained from the global fitting analysis of the data in panel A.

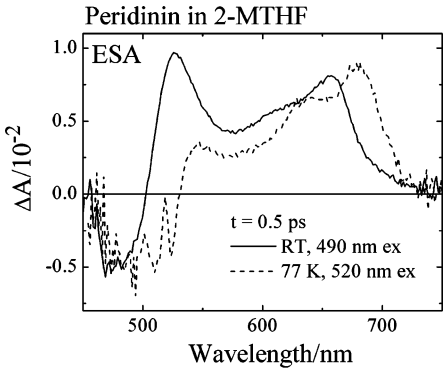

FIGURE 8: Transient absorption spectra of peridinin in 2-MTHF at room temperature (—) and 77 K (---) taken 0.5 ps after excitation at 490 and 520 nm, respectively.

for MFPCP and at 670 nm for HSPCP. This component was replaced in 5.5 ± 1 ps (MFPCP) or 23 ± 2 ps (HSPCP) with a nondecaying component. For the MFPCP complex (Figure 6A), the bleaching of the Chl Q_y band red-shifts by 1 nm in going from the first to the second EADS, whereas for HSPCP (Figure 6B), the bleaching shifts by 8 nm. This proves that upon excitation in the Chl Q_y band at 660 nm, energy is transferred from the short-wavelength-absorbing Chl to the long-wavelength-absorbing Chl in 5.5 ± 1 ps for the MFPCP and 23 ± 2 ps for the HSPCP. However, when the complexes were excited at 530 nm in the peridinin region, the Chl-to-Chl energy transfer times were found by the global fitting procedure to be slower; viz., 20 ± 5 ps for the MFPCP and 30 ± 2 ps for the HSPCP. The reason for this difference is not clear. There was no change in the spectra or dynamics brought about by increasing the pump laser intensity from 600 nJ to 2.0 μJ other than an increase in signal amplitude. The observation of a small positive amplitude in the 20 ps EADS component in the 600−650 nm region of peridinin excited-state absorption in the MFPCP (Figure 5A) suggests that some peridinin molecules may be transferring energy more slowly to Chl than when Chl is excited directly.

As a control, the excited-state absorption spectrum of peridinin was taken at room temperature and at 77 K in the moderately polar [$P(\epsilon) = 0.659$] solvent 2-MTHF (Figures 7 and 8). At room temperature (Figure 7A), at the earliest time delay, negative amplitude appears in the region 450−550 nm, corresponding to ground-state bleaching, and stimulated fluorescence and positive amplitude is seen above 650 nm, which is attributable to $S_2 \rightarrow S_n$ absorption. The EADS global fitting analysis (Figure 7B) suggests these features correspond to a 70 fs component. However, our instrument response time is no better than 130 fs. A value of 130 ± 10 fs was reported for the S_2 lifetime of peridinin in methanol (*13*). At longer (0.5−5.0 ps) delay times the characteristic two-signal excited-state spectrum of peridinin appears and persists for a few hundred picoseconds (Figure 7A). The EADS global fitting shows that a 4.2 ± 0.5 ps component loses part of its intensity at ~520 nm but gains intensity at ~650 nm as it decays into the longest-lived, 124 ± 10 ps, component. This behavior is explained by an equilibrium being established between the S_1 and S_{ICT} states after a few picoseconds. The global fitting of the present results in 2-MTHF indicate the equilibrium is established in 4.2 ± 0.5 ps and that the equilibrated $S_{1/ICT}$ system decays back to the ground state in 124 ± 10 ps.

Experiments on peridinin in 2-MTHF are valuable to the interpretation of the low-temperature excited-state spectral line shapes of the PCP complexes observed here because 2-MTHF is a moderately polar solvent that forms a clear glass when cooled below freezing. Figure 8 shows spectra taken at room temperature and 77 K at a 0.5 ps time delay overlaid to illustrate the changes in the excited-state absorption that accompany freezing. Upon lowering the temperature, there is a pronounced decrease in the intensity of the short (~520 nm) wavelength $S_1 \rightarrow S_n$ transition and a red shift and build-up of intensity associated with the $S_{ICT} \rightarrow S_n$ transition at longer (650−680 nm) wavelengths. Thus, lowering the temperature shifts the $S_1 \leftrightarrow S_{ICT}$ equilibrium toward the S_{ICT} state, suggesting this is the state from which energy is transferred to Chl at cryogenic temperatures.

DISCUSSION

Steady-State Spectra. The steady-state absorption spectra of the PCP complexes at 10 K exhibit vibronic structure in

the 400−600 nm peridinin absorption region not resolved in the spectra taken at room temperature (*4*). Reconstruction of the 10 K spectrum of the HSPCP complex by use of individual low-temperature absorption spectra from peridinin and Chl indicated that five of the peridinin molecules in the complex are spectrally equivalent and one is blue-shifted (*4*). In contrast, the spectral analysis of the 10 K steady-state absorption spectrum of the MFPCP required two blue-shifted peridinins and three separate pairs of peridinin spectra to fit its broader and less vibronically resolved spectrum shown in Figure 2 (*4*, *15*). These results suggest that the peridinins bound in the MFPCP complex are more energetically diverse in their binding sites compared to those in the HSPCP complex.

There can be many reasons why the peridinins bound in the pigment−protein complex absorb at different wavelengths. Differences in the structures of the peridinins or the polarity of the environment, excitonic coupling between pigments, or the presence of charged residues in proximity to the chromophores can all cause spectral shifts. The crystal structure of the MFPCP complex revealed that the eight bound peridinin molecules are not structurally equivalent (*5*). MNDO−PSDCI computations using the coordinates of the peridinin molecules from the crystal structure of the MFPCP complex examined the effect of conformational distortion on their absorption spectra (*15*). The calculations showed that six of the peridinin molecules in the MFPCP complex had spectra similar to that observed for isolated *all-trans*-peridinin. It was proposed that rotational distortion around polyene single bonds, which destabilizes the excited states more than the ground states, causes the blue shift. Moreover, the coordinates of Per612 and Per622 (Figure 1) showed these molecules to be significantly more distorted than the six other peridinins in the MFPCP. The computations suggested that these two peridinins have significantly blue-shifted spectra together with inverted S_1 and S_2 excited singlet states and that this inversion enhances energy transfer to the other peridinin molecules rather than directly to Chl (*15*).

Peridinin Spectral Properties. HSPCP lacks the peridinin equivalents of Per612 and Per622 in the MFPCP (Figure 1), yet analysis of the 10 K absorption spectrum of the HSPCP complex still requires one blue-shifted peridinin to account for its overall line shape (*4*). Molecular orbital computations reveal why this is the case. Each peridinin in the HSPCP was examined by MNDO−PSDCI methods, and all but one was revealed to have a small or negligible red shift. Peridinin PID-1329 was found to have a unique binding site that generates a 20−40 nm blue shift relative to the other peridinin chromophores. The origin of the blue shift is explored by first assuming that Glu-134 and Glu-136 are negatively charged and Lys-137 is positively charged (Figure 9). Glu-136 is the key residue responsible for the blue shift because of its close proximity (∼4.8 Å) to PID-1329. In the ground state, this residue creates a negatively charged region near the lactone ring end of the peridinin chromophore. The source of the blue shift then is the interaction of this negative charge with the electronic charge shift that accompanies excitation into the strongly allowed $^1B_u^+$-like state. This directs negative charge toward the lactone ring end of the chromophore (Figure 9). The static charge associated with Glu-136 and the charge shift upon excitation enhance electron−electron repulsion that increases the energy of the excited singlet state, resulting in a blue shift of approximately 20 nm. Because the binding sites of the remaining peridinin molecules have a net red-shifting or neutral impact, PID-1329 may be selectively blue-shifted by nearly 40 nm relative to the ensemble as experimentally observed (*4*).

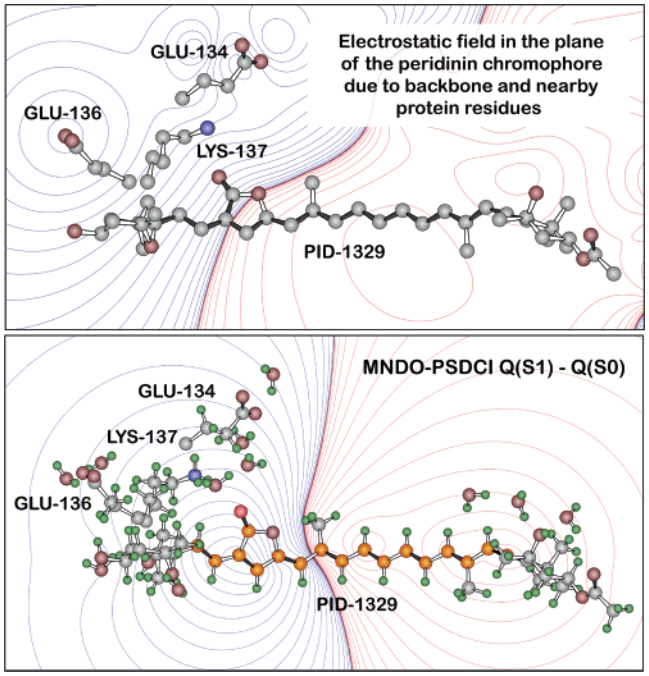

FIGURE 9: Ground and excitation-induced changes in electrostatic fields associated with peridinin, PID-1329. Blue lines indicate regions of excess negative charge, red lines indicate regions of excess positive charge, and the black line indicates neutrality. The low-lying strongly allowed absorption maximum is calculated to be at 438 nm, blue-shifted by at least 20−40 nm relative the other peridinin molecules, which have binding sites that are either neutral or red-shifting. The origin of the blue shift is Glu-136, which destabilizes the excited singlet state due to electron−electron repulsion of the electron charge-shift associated with excitation. Contours are drawn at the following energies (joules per mole): 0, ±0.5, ±3, ±10, ±23, ±45, ±79, ±125, ±186, ±265, ±363, ±484, ±628, ±799, ±997, ±1230, ±1490, ±1790, ±2120, ±2490, and ±2910.

Chlorophyll Spectral Properties. One of the most striking observations regarding the HSPCP complex is that the absorption spectrum in the region of the Chl Q_y transitions around 670 nm is split into two well-resolved bands at 10 K. An overlay of the 10 K absorption spectra of the MFPCP and HSPCP complexes reveals that one of the Chl Q_y bands in the HSPCP is significantly red-shifted while the other band remains close to the absorption wavelength of the Chls in the MFPCP complex (Figure 2). Interactions between charged amino acid side chains and Chl can cause shifts in the Q_y transition energies to either the red or blue depending on the sign and location of the charges relative to the direction of the ground- and excited-state dipole moments of the Chl (*47*−*49*).

It is interesting that the Q_y bands show a resolved splitting at low temperature but not at room temperature. However, the splitting is still present at room temperature, but it is not as readily observable due to inhomogeneous broadening of the Q_y system origin. There are many factors that can contribute to this spectral broadening at room temperature. First, thermal motion of the protein matrix will have an important impact. In addition, calculations indicate that the

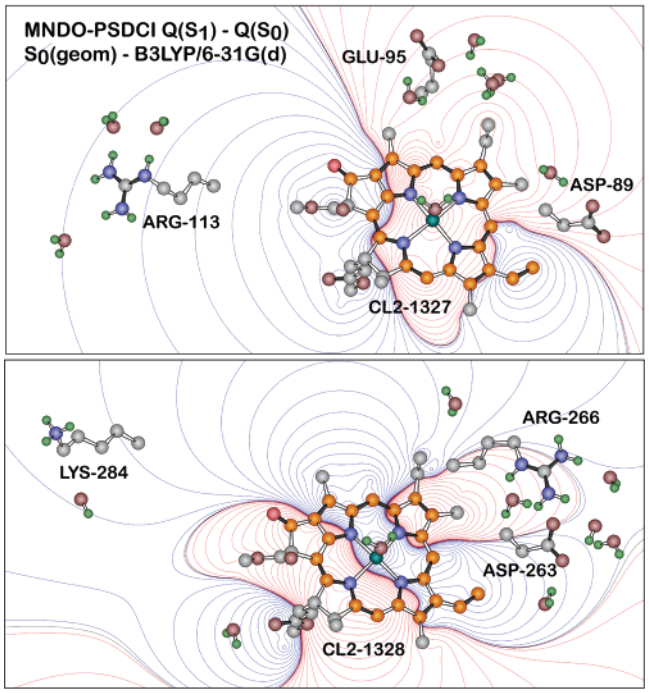

FIGURE 10: Charge shifts associated with excitations into the lowest-energy allowed singlet states of chlorophylls, CL2-1327 and CL2-1328. CL2-1327 is red-shifted by 16 nm relative to CL2-1328. This preferential red shift is due primarily to Arg-113, which provides significant electrostatic stabilization of the excited state. Note that, upon excitation, there are shifts of electron density in both chlorophylls toward the positively charged residues Arg-113 (top) or Lys-284 (bottom). These shifts of negative charge are stabilized by the positive charge, preferentially lowering the energy of the excited state and generating a red shift. The Arg-113 stabilization is more significant than Lys-284 because it is closer to the π-system of the chlorophyll. Contours are drawn at the following energies (joules per mole): 0, ±1, ±6, ±21, ±49, ±95, ±164, ±260, ±388, ±552, ±758, ±1010, ±1310, ±1660, ±2080, ±2560, ±3100, ±3720, ±4420, ±5200, and ±6060.

potential surface of out-of-plane torsion of the vinyl group on ring I is quite broad, and it is likely that this group is contributing to the inhomogeneous broadening at room temperature by sampling dihedral angles from 5° to 50°.

The key features of the binding sites of the two chlorophylls in HSPCP are examined in Figure 10. It should be noted that Figure 10 is somewhat misleading in that those residues above and to the right of the chlorophylls in this figure are above the plane of the chromophores by more than 12 Å and have only a modest impact on the spectral features. In contrast, Arg-113 (top) and Lys-284 (bottom) are nearly in the plane and within ~8 Å of the chromophores (Figure 10). Assuming these two residues are positively charged, both will induce a red shift in the lowest-lying Q_y band. The MNDO-PSDCI calculations predict the Q_y bands of Chl CL2-1327 at 691 nm ($f = 0.139$) and of Chl CL2-1328 at 675 nm ($f = 0.138$). The calculated splitting of 16 nm is in reasonable agreement with the experimentally observed splitting of 8 nm. The red shift associated with the Arg-113 (or Lys-284) is due to electrostatic stabilization of the excited state, quite the opposite to the situation examined for PID-1329 in Figure 9. In the present case, the two positively charged residues are helping to stabilize the shift of negative charge in their direction that accompanies excitation. In that regard, Arg-113 is more effective due to location and nature of the charge shift, as can be quantitatively compared on the basis of the contour maps shown in Figure 10.

Transient Absorption Spectra. The transient absorption spectrum of the MFPCP complex taken at 0.1 ps delay time shows a pronounced maximum at ~650 nm attributable to $S_{1/ICT} \rightarrow S_n$ absorption of peridinin (Figure 3A), whereas the transient absorption spectrum of the HSPCP at the same delay time (Figure 3B) is flatter and less intense in this region. This difference results from HSPCP having only six peridinins compared to eight in MFPCP and to the effect solvent polarity has on the peridinin excited-state absorption profiles (*22*). From previous work at room temperature, it is known that the $S_{1/ICT} \rightarrow S_n$ excited-state absorption spectrum of peridinin in moderately strong polar solvents, ethyl acetate [$P(\epsilon) = 0.626$] and 2-propanol [$P(\epsilon) = 0.852$], has peaks at ~520 and ~650 nm (*22*). As mentioned above, the short-wavelength peak is attributed to the familiar, strongly allowed $S_1 \rightarrow S_n$ absorption band seen in all carotenoids. The longer-wavelength intensity is assigned to a transition originating from the S_{ICT} state, which as shown in Figure 8 becomes stronger as the temperature is lowered. In MFPCP much of the excited-state absorption at 650 nm can be assigned to Per612 and Per622 that protrude into the intratrimer space (Figure 1) and presumably occupy a moderately polar binding site. Because HSPCP is monomeric and lacks these two peridinins, it has reduced excited-state absorption at 650 nm.

Peridinin-to-Chl Energy Transfer. Analysis of the excited-state absorption spectral data from the MFPCP and the HSPCP complexes suggests that, at very early times, energy is transferred from the peridinin S_2 state to Chl. This is shown by the instantaneous appearance of Q_y band bleaching in the transient spectra (Figure 3) and also by the appearance of negative Q_y band features in the earliest EADS components (Figure 5). The relative contribution (ϵ_2) from the S_2 state of peridinin to Chl to overall energy transfer can be calculated from the integrated areas of the Chl Q_y band bleaching of the first and fourth EADS components (Figure 5). The integrated area of the Chl Q_y bleaching observed in the first (<130 fs) EADS component is proportional to the amount of energy transferred directly from the S_2 state of peridinin. The fact that no significant change in the peridinin excited-state $S_{1/ICT} \rightarrow S_n$ absorption profile was observed in going from the fourth to the fifth EADS indicates that energy transfer from peridinin to Chl is complete during this time. Thus, the integrated area of the Chl Q_y bleaching of either the fourth or fifth EADS component will assess the total amount of energy transferred to Chl from all of the singlet states of peridinin. The ratio of the integrated areas of the Chl Q_y band bleaching obtained from the first and the fourth EADS yields the relative contribution of energy transferred from the S_2 state of peridinin to Chl. The contributions were found to be 22 ± 2% for the MFPCP and 11 ± 2% for the HSPCP. The value for the MFPCP complex determined here at 10 K is slightly below the range of 25−50% previously reported from room-temperature experiments (*7*, *8*, *13*), but given the difference in the temperature and uncertainty in the measurements, the present value is consistent with the published reports.

The excited-state absorption experiments on peridinin in 2-MTHF at 77 K (Figure 8) show that equilibration at low temperatures favors the S_{ICT} state over the S_1 state and suggests that in PCP at cryogenic temperatures the energy

Table 1: Time Constants of the Transient Absorption Data of MFPCP and HSPCP Taken at Room and Cryogenic Temperatures[a]

sample	temp	pump λ (nm)	τ_{ET2} (fs)	τ_{ET1}' (ps)	τ_{ET1} (ps)	$\tau_{Chl\text{-}Chl}$ (ps)	τ_{ND}	ref
MFPCP	RT	530	<130	0.6 ± 0.1	2.6 ± 0.2	36 ± 4	ND	this work
MFPCP	10 K	530	<130	0.4 ± 0.2	1.7 ± 0.2	20 ± 5	>740 ps	this work
MFPCP	10 K	660	na	na	na	5.5 ± 1	ND	this work
MFPCP	20 K	666	na	na	na	6.8	ND	*4*
HSPCP	RT	530	<130	0.8 ± 0.1	3.0 ± 0.2	45 ± 5	ND	this work
HSPCP	10 K	530	<130	0.5 ± 0.1	1.9 ± 0.2	30 ± 2	ND	this work
HSPCP	10 K	660	na	na	na	23 ± 2	ND	this work
HSPCP	20 K	666	na	na	na	20	ND	*4*
PCP	77 K	500	~100	nd	1.8	30 ± 5	>800 ps	*54*
PCP	77 K	520	~100	nd	1.8	60 ± 10	>300 ps	*54*
PCP	RT	535	<100	0.7 ± 0.1	2.5 ± 0.2	35 ± 5	3.7 ns	*8*
PCP	RT	500	~100	nd	2.3 ± 0.2	nd	>1000	*7*
PCP[b]	RT	530	180	nd	3.2 ± 0.3	46 ± 5	4.5 ± 0.1 ns	*6*
PCP	RT	510	nd	0.8	3.6-3.9	nd	3.7 ns	*13*
reconstituted PCP	RT	535	100 ± 25	0.6 ± 0.1	2.9 ± 0.3	25 ± 6	ND	*46*
PCP	RT	660	na	na	na	6.8 ± 0.8[b]	nd	*9*
PCP	RT	670	na	na	na	6.4	nd	*55*

[a] τ_{ET2}, τ_{ET1}', and τ_{ET1} are the energy transfer times from peridinin S_2, vibrationally hot S_1 and S_{ICT}, and S_{ICT} to Chl, respectively. $\tau_{Chl-Chl}$ is the energy transfer time from short-wavelength-absorbing Chl to long-wavelength-absorbing Chl. τ_{ND} represents the lifetime of Chl *a* excited state. ND, nondecaying; na, not applicable; nd, not detected. All time constants were obtained by global fitting except as noted. [b] Obtained by single-wavelength fitting analysis rather than global fitting. [c] Value obtained from time-resolved fluorescence anisotropy spectroscopy.

donor state to Chl is S_{ICT}. The energy transfer efficiency, ϵ_1, from the S_{ICT} state to Chl can be obtained from the equation $\epsilon = \epsilon_1(100 - \epsilon_2)/100 + \epsilon_2$ if the overall energy transfer efficiency, ϵ, from peridinin to Chl is known. The overall peridinin-to-Chl energy transfer efficiency has been obtained from fluorescence excitation measurements and found to be >95% for both the MFPCP and the HSPCP complexes (*4*). From this value of ϵ and the values of ϵ_2 determined above, the energy transfer efficiency from the S_{ICT} state of peridinin is found to be >94% for both MFPCP and HSPCP complexes. Thus, the major part of the excited-state population arrives in the S_1 and S_{ICT} states via internal conversion from S_2, but low temperatures favor the S_{ICT} state, which transfers its energy to Chl.

The increased bleaching of the Chl Q_y bands between 130 fs and 0.5 ps times after excitation suggests energy transfer may occur from vibrationally hot S_1 or S_{ICT}. The energy transfer efficiency of this process was determined by integrating the areas of the Chl Q_y band bleaching of the second EADS component (Figure 5). As mentioned above, the integral of the first EADS component is proportional to the amount of energy transferred directly from the peridinin S_2 state. The integral of the second EADS component in the Q_y region indicates the amount of energy transferred from the S_2 and vibrationally hot S_1 and S_{ICT} states of peridinin. The difference in the integrated areas of the first and second EADS is therefore proportional to the amount of energy transferred from vibrationally hot S_1 and S_{ICT}. The ratio of this difference and the fourth EADS integrated areas gives the energy transfer efficiency from the vibrationally hot S_1 and S_{ICT} to Chl, which was found to be 24 ± 5% for both MFPCP and HSPCP complexes.

Direct kinetics measurements provide an alternative manner in which to determine the energy transfer efficiencies, ϵ_1 and ϵ_2. The relevant equations are and

$$\epsilon_1 = \frac{k_{ET1}}{(k_{ET1} + k_{IC1})} \times 100\% \quad (1)$$

$$\epsilon_2 = \frac{k_{ET2}}{(k_{ET2} + k_{IC2})} \times 100\% \quad (2)$$

where k_{ET1} and k_{ET2} are the rate constants for energy transfer from the S_{ICT} and S_2 states of peridinin and k_{IC1} and k_{IC2} are the rate constants for internal conversion from the S_{ICT} and S_2 states. This assumes that both the rate constant for internal conversion from S_2 and the rate constant for S_{ICT} population from S_1 are very large compared to k_{ET1}. The energy transfer time, $\tau_{ET1} = 1/k_{ET1}$, from the S_{ICT} state of peridinin was found from the global fitting analysis (Figure 5) to be 1.7 ± 0.2 ps for the MFPCP complex and 1.9 ± 0.2 ps for HSPCP (Table 1). For comparison with the data taken on the complexes at low temperatures, the intrinsic S_{ICT} lifetime, $\tau_{IC1} = 1/k_{IC1}$, of peridinin in the absence of energy transfer to Chl, was measured in 2-MTHF solvent at 77 K to be 160 ± 10 ps (data not shown). Zigmantas et al. (*25*) reported this lifetime of peridinin in an ethylene glycol glass at 77 K to be 206 ± 21 ps. Either of these numbers yields an ϵ_1 value of >99% from eq 1 for the MFPCP and the HSPCP complexes. This is consistent with the statement above that the majority of population arriving in the S_{ICT} state from the S_2 state of peridinin is transferred to Chl.

The time constant for energy transfer from the S_2 state of peridinin in both complexes was either comparable to or shorter than the instrument response time. Thus, it is not possible to use eq 2 to verify, from the present data, consistency with the 25−50% values previously reported (*7*, *8*, *13*).

Chl-to-Chl Energy Transfer. Direct excitation of the short-wavelength-absorbing Chl into its Q_y band at 660 nm results in energy transfer to the long-wavelength-absorbing Chl as seen in Figure 6. This transfer time is observed to be 23 ± 2 ps for the HSPCP complex compared to 5.5 ± 1 ps for the MFPCP, that is, a factor of 4.2 slower in the HSPCP. The rate constant for energy transfer between the Chls is determined by three primary factors: distance, orientation, and spectral overlap as described by Förster (*50*). According to this model, the rate constant, k_{DA}, for energy transfer from a donor, D, to an acceptor, A, is

$$k_{DA} = c\frac{\kappa^2 k_r^D}{r^6 n^4}\int\frac{\epsilon_A(\tilde{\nu})f_D(\tilde{\nu})}{\tilde{\nu}^4}\,d\tilde{\nu} \quad (3)$$

where c is a constant, κ is the orientation factor between dipoles, k_r^D is the radiative rate constant of the energy donor, r is the center-to-center distance between the molecules, n is the refractive index of the medium, ϵ_A corresponds to the absorption of the acceptor on a wavenumber (cm^{-1}) scale, and f_D represents the fluorescence spectrum of the donor also on a wavenumber scale. The term κ is

$$\kappa = \vec{\mu}_D\cdot\vec{\mu}_A - 3(\vec{\mu}_D\cdot\vec{r}_{DA})(\vec{\mu}_A\cdot\vec{r}_{DA}) \quad (4)$$

where $\vec{\mu}_D$ and $\vec{\mu}_A$ are the transition moment unit vectors for the donor and acceptor molecules, respectively, and $\vec{r}_{DA}$ is the unit vector in the direction of the line connecting centers of the two molecules.

The crystal structures of the complexes can be used to elucidate which factors are responsible for the change in energy transfer time. From the crystalline coordinates, the center-to-center distance between the two Chls was found to be 17.4 Å in the MFPCP complex and 18.4 Å in the HSPCP. Substituting these values of r into eq 3 while keeping other parameters constant for both complexes yielded a MFPCP:HSPCP ratio of rate constants of energy transfer from Chl-to-Chl of 1.4. Therefore, distance can account for only part of the factor of 4.2 difference in rate constant.

The parameter κ characterizing the orientation of the donor and acceptor Chl Q_y transition dipoles was calculated from eq 4 for both complexes, with the assumption that the Q_y transition moments of the two Chls (denoted Chl601 and Chl602 in the MFPCP structure and CL2-1327 and CL2-1328 in the HSPCP) are represented by unit vectors connecting the nitrogen atoms in pyrrole rings I and III of the Chl *a* macrocycles. For the MFPCP complex, the coordinates of the nitrogens labeled N2316 and N2300 of Chl601 and N2381 and N2365 of Chl602 were used. For the HSPCP, the unit vectors were determined from the coordinates of nitrogen atoms N2378 and N2394 of CL2-1327 and N2443 and N2459 of CL2−1328. The unit vector $\vec{r}_{DA}$ was calculated from the coordinates of the two Mg centers of the Chls. The calculated κ values were −0.394 for the MFPCP complex and −0.417 for the HSPCP complex. The κ values computed in this manner assume fixed transition dipole moments, but small environmental perturbations can shift these values to both increase and decrease the coupling, which is assumed to be the same in comparing the main-form and high-salt PCP, which have nearly identical Chls. On the basis of this difference in κ, and keeping the other parameters constant, the ratio of the rate constants of Chl-to-Chl energy transfer for the MFPCP and HSPCP was found to be 0.9. Thus, the orientation factor predicts a slightly slower energy transfer rate constant for MFPCP than for HSPCP, which is not observed.

The combined effects of distance and orientation account for only a factor of 1.3 difference in the rate constant for energy transfer and therefore are not sufficient to account for the factor of 4.2. The remaining factor of 4.2/1.3 = 3.2 in the ratio may arise from differences in spectral overlap between the donor Chl emission and acceptor Chl absorption. The ratio of the spectral overlap integrals of the MFPCP and HSPCP complexes can be computed in two ways: (1) by use of the absorption and emission spectra of purified Chl in 2-MTHF (*4*) and (2) by use of the actual emission and absorption spectra of the complexes. Both approaches have shortcomings because assumptions need to be made regarding the wavelength positions of the donor emission bands.

In computing the spectral overlap by use of the Chl absorption and emission spectra in 2-MTHF taken at 77 K, for the MFPCP, the maximum of the emission spectrum was positioned at 666 nm, corresponding to where the short-wavelength-absorbing Chl donor emission is most likely to occur. The position of the long-wavelength-absorbing Chl acceptor maximum was set at 667 nm. For HSPCP, the maxima of the emission spectrum of the short-wavelength-absorbing Chl donor and the absorption spectrum of the long-wavelength-absorbing Chl acceptor were set at 668 and 676 nm, respectively. This yielded a MFPCP:HSPCP spectral overlap ratio of 1.4 (*4*).

In the second approach, the spectral overlap was computed by use of the emission and absorption spectra of Chl *a* in the actual MFPCP and HSPCP complexes. For the MFPCP complex, the emission spectrum of the Chl donor was assumed to have a maximum at 669 nm and the absorption spectrum of the Chl acceptor was placed at 670 nm, corresponding to the positions of the bleaching of the two Chls from the EADS global fitting analysis (Figure 6). A similar procedure was carried out for the HSPCP complex, where the maxima of the emission spectrum of the donor Chl and the absorption spectrum of the acceptor Chl were positioned at 670 and 678 nm, respectively. The ratio of the spectral overlap integrals of the MFPCP and HSPCP complexes computed in this manner was 2.6. Thus, for either method of computing spectral overlap, the combined distance/orientation/spectral overlap factors, 1.4 × 0.9 × (1.4−2.6) = 1.8−3.3, still cannot account for the entire factor of 4.2 difference in Chl-to-Chl energy transfer rate constant observed for the MFPCP compared to the HSPCP complex.

A major difference in the structure of HSPCP versus MFPCP is the fact that Per612 and Per622 occupy the region between the Chls. In the HSPCP, these peridinins are absent and the space is filled by phytol tails of CL2-1327 and CL2-1328. This alteration in the structures between MFPCP and HSPCP can affect the rate constant of Chl-to-Chl energy transfer. It has been reported that carotenoids in the LH2 light-harvesting complex from purple photosynthetic bacteria act as bridging polarizable units that can perturb the transition densities of both the B800 and B850 BChls and enhance the rate of energy transfer between them (*51*, *52*). The presence of carotenoids was postulated to mediate the coupling between B800 and B850 BChls through an indirect, superexchange mechanism (*51*, *52*). Another study on the effect of a bridging medium on the energy transfer rate between π-electron donors and acceptors was reported on porphyrin dimers having different linkages; viz., bicyclo-[2.2.2]octane, benzene, naphthalene, and anthracene (*53*). The measured energy transfer rate constant between the porphyrin dimers was $3.7 \times 10^8\ s^{-1}$ when bicyclo[2,2,2]octane, which does not have a conjugated π-electronic system, was used as the bridging molecule, and the value increased to $4.8 \times 10^8\ s^{-1}$, $5.3 \times 10^8\ s^{-1}$, and $12.1 \times 10^8\ s^{-1}$ when benzene, naphthalene, and anthracene were present, respectively (*53*). This work proposed that the observed increase in energy

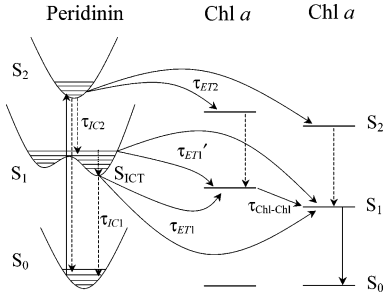

FIGURE 11: Schematic diagram of the peridinin-to-Chl and Chl-to-Chl energy transfer for both MFPCP and HSPCP complexes. Energy transfer times are represented for all the active pathways. The values are given in Table 1.

transfer rate constant was due to alterations in electronic coupling between the donor and acceptor (*53*). These data prove that a bridging molecule (e.g., Per612 and Per622) having a conjugated π-electronic system can significantly enhance the energy transfer rate constant and may well account for the enhanced rate of Chl-to-Chl energy transfer in MFPCP compared to HSPCP.

Energy Transfer Scheme. A schematic diagram that summarizes the pathways for peridinin-to-Chl and Chl-to-Chl energy transfer for the MFPCP and HSPCP complexes at low temperatures is shown in Figure 11. Upon excitation of the complexes in the peridinin absorption region, peridinin is promoted to the S_2 state, and some population is transferred in less than 130 fs from the S_2 state to both Chls. After internal conversion from the S_2 state to the S_1 and S_{ICT} states of peridinin, which favors the S_{ICT} state at low temperatures, energy is transferred with very similar rates to both Chls. The short-wavelength-absorbing Chl then transfers energy to the long-wavelength-absorbing Chl, where it is made available for use in driving the primary photochemical redox reactions of photosystem II.

ACKNOWLEDGMENT

We thank Dr. Eckhard Hofmann for providing valuable information regarding the crystal structure of the HSPCP complex and Drs. Tomáš Polívka and Robert Knox for helpful discussions.

REFERENCES

1. Song, P.-S., Koka, P., Prézelin, B. B., and Haxo, F. T. (1976) Molecular topology of the photosynthetic light-harvesting pigment complex, peridinin−chlorophyll *a*−protein, from marine dinoflagellates, *Biochemistry 15*, 4422−4427.
2. Koka, P., and Song, P.-S. (1977) The chromophore topography and binding environment of peridinin−chlorophyll *a*−protein complexes from marine dinoflagellate algae, *Biochim. Biophys. Acta 495*, 220−231.
3. Akimoto, S., Takaichi, S., Ogata, T., Nishimura, Y., Yamazaki, I., and Mimuro, M. (1996) Excitation energy transfer in carotenoid−chlorophyll protein complexes probed by femtosecond fluorescence decays, *Chem. Phys. Lett. 260*, 147−152.
4. Ilagan, R. P., Shima, S., Melkozernov, A., Lin, S., Blankenship, R. E., Sharples, F. P., Hiller, R. G., Birge, R. R., and Frank, H. A. (2004) Spectroscopic properties of the main-form and high-salt peridinin−chlorophyll *a* proteins from *Amphidinium carterae*, *Biochemistry 43*, 1478−1487.
5. Hofmann, E., Wrench, P. M., Sharples, F. P., Hiller, R. G., Welte, W., and Diederichs, K. (1996) Structural basis of light harvesting by carotenoids: Peridinin−chlorophyll−protein from *Amphidinium carterae*, *Science 272*, 1788−1791.
6. Bautista, J. A., Hiller, R. G., Sharples, F. P., Gosztola, D., Wasielewski, M., and Frank, H. A. (1999) Singlet and triplet energy transfer in the peridinin−chlorophyll *a*−protein from *Amphidinium carterae*, *J. Phys. Chem. A 103*, 2267−2273.
7. Krueger, B. P., Lampoura, S. S., van Stokkum, I. H. M., Papagiannakis, E., Salverda, J. M., Gradinaru, C. C., Rutkauskas, D., Hiller, R. G., and van Grondelle, R. (2001) Energy transfer in the peridinin chlorophyll *a* protein of *Amphidinium carterae* studied by polarized transient absorption and target analysis, *Biophys. J. 80*, 2843−2855.
8. Zigmantas, D., Hiller, R. G., Polivka, T., and Sundström, V. (2002) Carotenoid to chlorophyll energy transfer in the peridinin chlorophyll-*a* protein complex: A unique pathway involving an intramolecular charge transfer state, *Proc. Natl. Acad. Sci. U.S.A. 99*, 16760−16765.
9. Kleima, F. J., Hofmann, E., Gobets, B., Van Stokkum, I. H. M., Van Grondelle, R., Diederichs, K., and Van Amerongen, H. (2000) Förster excitation energy transfer in peridinin−chlorophyll-*a*−protein, *Biophys. J. 78*, 344−353.
10. Kleima, F. J., Wendling, M., Hofmann, E., Peterman, E. J. G., van Grondelle, R., and van Amerongen, H. (2000) Peridinin chlorophyll *a* protein: Relating structure and steady-state spectroscopy, *Biochemistry 39*, 5184−5195.
11. Krikunova, M., Lokstein, H., Leupold, D., Hiller, R. G., and Voigt, B. (2006) Pigment−pigment interactions in PCP of *Amphidinium carterae* investigated by nonlinear polarization spectroscopy in the frequency domain, *Biophys. J. 90*, 261−271.
12. Lampoura, S. S., Krueger, B. P., van Stokkum, I. H., Salverda, J. M., Gradinaru, C. C., Rutkauskas, D., Hiller, R. G., and van Grondelle, R. (2001) Energy transfer in the peridinin chlorophyll *a* protein of *Amphidinium carterae* studied by polarized absorption measurements, *Int. J. Mod. Phys. B 15*, 3849−3852.
13. Linden, P. A., Zimmermann, J., Brixner, T., Holt, N. E., Vaswani, H. M., Hiller, R. G., and Fleming, G. R. (2004) Transient absorption study of peridinin and peridinin chlorophyll *a* protein after two-photon excitation, *J. Phys. Chem. B. 108*, 10340−10345.
14. Zimmermann, J., Linden, P. A., Vaswani, H. M., Hiller, R. G., and Fleming, G. R. (2002) Two-photon excitation study of peridinin in benzene and in the peridinin chlorophyll *a*−protein (PCP), *J. Phys. Chem. B 106*, 9418−9423.
15. Shima, S., Ilagan, R. P., Gillespie, N., Sommer, B. J., Hiller, R. G., Sharples, F. P., Frank, H. A., and Birge, R. R. (2003) Two-photon and fluorescence spectroscopy and the effect of environment on the photochemical properties of peridinin in solution and in the peridinin−chlorophyll−protein from *Amphidinium carterae*, *J. Phys. Chem. A 107*, 8052−8066.
16. Vaswani, H. M., Hsu, C. P., Head-Gordon, M., and Fleming, G. R. (2003) Quantum chemical evidence for an intramolecular charge-transfer state in the carotenoid peridinin of peridinin−chlorophyll−protein, *J. Phys. Chem. B 107*, 7940−7946.
17. Carbonera, D., Giacometti, G., Segre, U., Hofmann, E., and Hiller, R. G. (1999) Structure-based calculations of the optical spectra of the light-harvesting peridinin−chlorophyll−protein complexes from *Amphidinium carterae* and *Heterocapsa pygmaea*, *J. Phys. Chem. B 103*, 6349−6356.
18. Ritz, T., Damjanovic, A., Schulten, K., Zhang, J.-P., and Koyama, Y. (2000) Efficient light harvesting through carotenoids, *Photosynth. Res. 66*, 125−144.
19. Damjanovic, A., Ritz, T., and Schulten, K. (2000) Excitation transfer in the peridinin−chlorophyll−protein of *Amphidinium carterae*, *Biophys. J. 79*, 1695−1705.
20. Sharples, F. P., Wrench, P. M., Ou, K., and Hiller, R. G. (1996) Two distinct forms of the peridinin−chlorophyll *a*−protein from *Amphidinium carterae*, *Biochim. Biophys. Acta 1276*, 117−123.
21. Liaaen-Jensen, S. (1971) in *Carotenoids* (Isler, O., Gutmann, H., and Solms, U., Eds.) pp 163, Birkhäuser Verlag, Basel, Switzerland.
22. Bautista, J. A., Connors, R. E., Raju, B. B., Hiller, R. G., Sharples, F. P., Gosztola, D., Wasielewski, M. R., and Frank, H. A. (1999) Excited-state properties of peridinin: Observation of a solvent dependence of the lowest excited singlet state lifetime and spectral behavior unique among carotenoids, *J. Phys. Chem. B 103*, 8751−8758.
23. Frank, H. A., Bautista, J. A., Josue, J., Pendon, Z., Hiller, R. G., Sharples, F. P., Gosztola, D., and Wasielewski, M. R. (2000) Effect of the solvent environment on the spectroscopic properties and dynamics of the lowest excited states of carotenoids, *J. Phys. Chem. B 104*, 4569−4577.
24. Zigmantas, D., Polivka, T., Hiller, R. G., Yartsev, A., and Sundström, V. (2001) Spectroscopic and dynamic properties of

the peridinin lowest singlet excited states, *J. Phys. Chem. A 105*, 10296−10306.
25. Zigmantas, D., Hiller, R. G., Yartsev, A., Sundström, V., and Polivka, T. (2003) Dynamics of excited states of the carotenoid peridinin in polar solvents: Dependence on excitation wavelength, viscosity, and temperature, *J. Phys. Chem. B 107*, 5339−5348.
26. DeCoster, B., Christensen, R. L., Gebhard, R., Lugtenburg, J., Farhoosh, R., and Frank, H. A. (1992) Low-lying electronic states of carotenoids, *Biochim. Biophys. Acta 1102*, 107−114.
27. Christensen, R. L., Goyette, M., Gallagher, L., Duncan, J., DeCoster, B., Lugtenburg, J., Jansen, F. J., and Hoef, I. v. d. (1999) S_1 and S_2 states of apo- and diapocarotenes, *J. Phys. Chem. A 103*, 2399−2407.
28. Andersson, P. O., Bachilo, S. M., Chen, R.-L., and Gillbro, T. (1995) Solvent and temperature effects on dual fluorescence in a series of carotenes. Energy gap dependence of the internal conversion rate, *J. Phys. Chem. 99*, 16199−16209.
29. Gillbro, T., Andersson, P. O., Liu, R. S. H., Asato, A. E., Takaishi, S., and Cogdell, R. J. (1993) Location of the carotenoid $2A_g^-$ state and its role in photosynthesis, *Photochem. Photobiol. 57*, 44−48.
30. Bondarev, S. L., and Knyukshto, V. N. (1994) Fluorescence from the S_1 (2^1A_g) state of all-trans-*b*-carotene, *Chem. Phys. Lett. 225*, 346−350.
31. Mimuro, M., Nagashima, U., Nagaoka, S., Takaichi, S., Yamazaki, I., Nishimura, Y., and Katoh, T. (1993) Direct measurement of the low-lying singlet excited (2^1A_g) state of a linear carotenoid, neurosporene, in solution, *Chem. Phys. Lett. 204*, 101−105.
32. Fujii, R., Onaka, K., Kuki, M., Koyama, Y., and Watanabe, Y. (1998) The $2A_g^-$ energies of all-trans-neurosporene and spheroidene as determined by fluorescence spectroscopy, *Chem. Phys. Lett. 288*, 847−853.
33. Mimuro, M., Nagashima, U., Nagaoka, S., Nishimura, Y., Takaichi, S., Katoh, T., and Yamazaki, I. (1992) Quantitative analysis of the solvent effect on the relaxation processes of carotenoids showing dual emissive characteristics, *Chem. Phys. Lett. 191*, 219−224.
34. Papagiannakis, E., Larsen, D. S., van Stokkum, I. H. M., Vengris, M., Hiller, R. G., and van Grondelle, R. (2004) Resolving the excited-state equilibrium of peridinin in solution, *Biochemistry 43*, 15303−15309.
35. Ilagan, R. P., Christensen, R. L., Chapp, T. W., Gibson, G. N., Pascher, T., Polivka, T., and Frank, H. A. (2005) Femtosecond time-resolved absorption spectroscopy of astaxanthin in solution and in a-crustacyanin, *J. Phys. Chem. A 109*, 3120−3127.
36. Linnanto, J., and Korppi-Tommola, J. (2004) Semiempirical PM5 molecular orbital study on chlorophylls and bacteriochlorophylls: Comparison of semiempirical, ab initio, and density functional results, *J. Comput. Chem. 25*, 123−138.
37. Brückner, C., Foss, P. C., Sullivan, J. O., Pelto, R., Zeller, M., Birge, R. R., and Crundwell, G. (2006) Origin of the bathochromically shifted optical spectra of meso-tetrathien-2′- and 3′-ylporphyrins as compared to meso-tetraphenylporphyrin, *Phys. Chem. Chem. Phys. 8*, 2402−12.
38. Brückner, C., McCarthy, J. R., Daniell, H. W., Pendon, Z. D., Ilagan, R. P., Francis, T. M., Ren, L., Birge, R. R., and Frank, H. A. (2003) A spectroscopic and computational study of the singlet and triplet excited states of synthetic β-functionalized chlorins, *Chem. Phys. 294*, 285−303.
39. Frisch, M. J., Trucks, G. W., Schlegel, H. B., Scuseria, G. E., Robb, M., Cheeseman, J. R., Montgomery, J. A., Jr., Vreven, T., Kudin, K. N., Burant, J. C., Millam, J. M., Iyengar, S. S., Tomasi, J., Barone, V., Mennucci, B., Cossi, M., Scalmani, G., Rega, N., Petersson, G. A., Nakatsuji, H., Hada, M., Ehara, M., Toyota, K., Fukuda, R., Hasegawa, J., Ishida, M., Nakajima, T., Honda, Y., Kitao, O., Nakai, H., Klene, M., Li, X., Knox, J. E., Hratchian, H. P., Cross, J. B., Adamo, C., Jaramillo, J., Gomperts, R., Stratmann, R. E., Yazyev, O., Austin, A. J., Cammi, R., Pomelli, C., Ochterski, J., Ayala, P. Y., Morokuma, K., Voth, G. A., Salvador, P., Dannenberg, J. J., Zakrzewski, V. G., Dapprich, S., Daniels, A. D., Strain, M. C., Farkas, O., Malick, D. K., Rabuck, A. D., Raghavachari, K., Foresman, J. B., Ortiz, J. V., Cui, Q., Baboul, A. G., Clifford, S., Cioslowski, J., Stefanov, B. B., Liu, G., Liashenko, A., Piskorz, P., Komaromi, I., Martin, R. L., Fox, D. J., Keith, T. A., Al-Laham, M. A., Peng, C. Y., Nanayakkara, A., Challacombe, M., Gill, P. M. W., Johnson, B., Chen, W., Wong, M. W., Gonzalez, C., and Pople, J. A. (2003) *Gaussian 03*, revision B. 04, Gaussian Inc., Pittsburgh, PA.
40. Vreven, T., Morokuma, K., Farkas, O., Schlegel, H. B., and Frisch, M. J. (2003) Geometry optimization with QM/MM, ONIOM, and other combined methods. I. Microiterations and constraints, *J. Comput. Chem. 24*, 760−769.
41. Vreven, T., and Morokuma, K. (2003) Investigation of the $S_0 \rightarrow S_1$ excitation in bacteriorhodopsin with the ONIOM(MO:MM) hybrid method, *Theor. Chem. Acc. 109*, 125−132.
42. Dolan, P. M., Miller, D., Cogdell, R. J., Birge, R. R., and Frank, H. A. (2001) Linear dichroism and the transition dipole moment orientation of the carotenoid in the LH2 antenna complex in membranes of *Rhodopseudomonas acidophila* strain 10050, *J. Phys. Chem. B 105*, 12134−12142.
43. Ren, L., Martin, C. H., Wise, K. J., Gillespie, N. B., Luecke, H., Lanyi, J. K., Spudich, J. L., and Birge, R. R. (2001) Molecular mechanism of spectral tuning in sensory rhodopsin II, *Biochemistry 40*, 13906−13914.
44. Martin, C. H., and Birge, R. R. (1998) Reparametrizing MNDO for excited-state calculations by using ab initio effective Hamiltonian theory: Application to the 2,4-pentadien-1-iminium cation, *J. Phys. Chem. A 102*, 852−860.
45. van Stokkum, I. H. M., Larsen, D. S., and van Grondelle, R. (2004) Global and target analysis of time-resolved spectra, *Biochim. Biophys. Acta 1657*, 82−104.
46. Polívka, T., Pascher, T., Sundstrom, V., and Hiller, R. G. (2005) Tuning energy transfer in the peridinin−chlorophyll complex by reconstitution with different chlorophylls, *Photosynth. Res. 86*, 217−227.
47. Gudowska-Nowak, E., Newton, M. D., and Fajer, J. (1990) Conformational and environmental effects on bacteriochlorophyll optical spectra: correlations of calculated spectra with structural results, *J. Phys. Chem. 94*, 5795−5801.
48. Eccles, J., and Honig, B. (1983) Charged amino acids as spectroscopic determinants for chlorophyll in vivo, *Proc. Natl. Acad. Sci. U.S.A 80*, 4959−4962.
49. Hanson, L. K., Fajer, J., Thompson, M. A., and Zerner, M. C. (1987) Electrochromic effects of charge separation in bacterial photosynthesis: theoretical models, *J. Am. Chem. Soc. 109*, 4728−4730.
50. Förster, T. (1968) Intermolecular energy transfer and fluorescence, *Ann. Phys. 2*, 55−75.
51. Krueger, B. P., Scholes, G. D., Gould, I. R., and Fleming, G. R. (1999) Carotenoid mediated B800−B850 coupling in LH2, *Phys. Chem. Commun. 2*, 34−40.
52. Scholes, G. D., and Fleming, G. R. (2000) On the mechanism of light harvesting in photosynthetic purple bacteria: B800 to B850 energy transfer, *J. Phys. Chem. B 104*, 1854−1868.
53. Kilsa, K., Kajanus, J., Martensson, J., and Albinsson, B. (1999) Mediated electronic coupling: singlet energy transfer in porphyrin dimers enhanced by the bridging chromophore, *J. Phys. Chem. B 103*, 7329−7339.
54. Lampoura, S. S. (2001) Vrije Universiteit, Amsterdam.
55. Salverda, J. M. (2003) Vrije Universiteit, Amsterdam.

BI061217U